Power Loss and Thermal Analysis of a MW High Speed Permanent Magnet Synchronous Machine

Yue Zhang, *Student Member, IEEE*, Sean McLoone, *Senior Member, IEEE*, Wenping Cao *Senior Member, IEEE*, Fengyi Qiu, and Chris Gerada, *Member, IEEE*

***Abstract*--High speed permanent magnet synchronous machines (PMSMs) have attracted much attention due to their high power density, high efficiency, and compact size for direct-drive applications. However, the consequent power loss density is high and heat transfer is also deemed as a technical challenge. This is particularly the case for high-speed operation. In this paper, electromagnetic and mechanical power losses in a MW level high speed PMSM is comprehensively investigated by finite element analysis; the transient machine demagnetization performance is studied with the proposed rotor composite structure to improve the machine anti-demagnetization capability; the temperature distribution of the high speed PMSM is also analyzed by a fluid-thermal coupling method with calculated power loss. The high speed PMSM is prototyped and experimentally tested to validate the effectiveness of numerical models and calculated results.**

***Index Terms*--Demagnetization, finite element method, High speed PM machine, magnetic field, power loss, thermal analysis.**

I. Introduction

HIGH speed permanent magnet synchronous machines (PMSMs) are increasingly popular owing to their excellent performance in industrial applications such as gas compressors, distributed power generation, electrical turbocharging, turbines and flywheel energy storage system [1]-[3]. Generally, these machines can be characterized as high power density, compact size, high reliability and suitability for direct-drive applications without gearboxes. Moreover, the PM machine is also favorable due to its remarkable performance in efficiency when compared with its induction and reluctance motor counterparts for high speed operation.

However, high speed rotation also results in some characteristic issues for PMSMs. High power density would cause high power loss density. Due to the high frequency magnetic alternating in the steel core lamination, the iron loss can be significantly high as it is closely relative to the power frequency [4]. Particularly, the rotor eddy current loss is of great importance as such loss heats the rotor directly [5]. Furthermore, rotor overheating may reduce machine performance and lead to the demagnetization of magnets. High speed PM machines have a smaller size than conventional machines and the rotor cooling can only be performed through the air gap [6]. Therefore, thermal transfer poses a particular challenge for high speed machines.

Heat losses of the high speed electrical machine reduce efficiency and cause temperature rise. Conventionally, the PM machine iron loss can be predicted by the Bertotti iron loss model [7] with an improvement to consider the rotational flux [8]-[10]. The iron loss of an interior PMSM under a flux-weakening region is studied in [11] by employing variable iron loss coefficients. A systematic analytical method to predict eddy current loss in both surface-mounted PM and rotor container sleeve is illustrated in [12]. The eddy current loss due to armature reaction field is presented analytically in [13] with equivalent current sheet distributed over stator slot openings but the slot effect is neglected. Finite Element Method (FEM) is widely adopted to study eddy current loss. Several methods to reduce rotor eddy current loss are proposed, such as copper layer plating on the rotor alloy sleeve outer surface [14] or rotor sleeve grooving [15]. Demagnetization is discussed for PM machine in [16]. However, it is only partially studied based on the PM surface flux density without considering the whole PM demagnetization and its effect on machine performance. Electrical and thermal analysis for high speed machine is also extensively researched. The time saving Lumped parameter thermal network (LPTN) is utilized in [17], and Computational fluid dynamics (CFD) method is well developed to improve the prediction precision [2] [6] [18].

In this paper, a MW level high speed PMSM is designed and investigated with its electromagnetic and mechanical power loss analyzed. The iron loss is estimated with an

This work was supported in part by the Royal Society, UK and by the National Natural Science Foundation, China under Grant 5141101208.

Yue Zhang and Sean McLoone are with the School of Electronics, Electrical Engineering and Computer Science, Queens University Belfast, Belfast, BT9 5AH UK (e-mail: yzhang35@ qub.ac.uk; s.mcloone@qub.ac.uk).

Wenping Cao is with Power Electronics, Machines and Power System Group, Aston University, Birmingham, B4 7ET UK (e-mail: w.p.cao@aston.ac.uk).

Fengyi Qiu is with Jiangsu Aerospace Power Electric Co., Ltd, Jingjiang, China (e-mail: qiufengyi163@163.com).

Chris Gerada is with Department of Electrical and Electronic Engineering, University of Nottingham, Nottingham, NG7 2RD UK (e-mail: chris.gerada@nottingham .ac.uk).

improved method considering harmonics and rotational magnetic flux effects. The machine stator structure and rotor sleeve are researched and studied by FEM to decrease rotor eddy current loss. The demagnetization behavior for the high speed PMSM with overload is studied. While composite rotor structure is also proposed and investigated to improve the machine anti-demagnetization capability in harsh conditions. Then the temperature distribution for the high speed machine is evaluated based on power loss and fluid-thermal coupling analysis. Finally the high speed PMSM is prototyped and experimentally tested for validation purposes.

II. High Speed PMSM Design

The design of high speed PMSMs is more complicated than a conventional machine, as their electromagnetic, thermal and mechanical aspects should all be considered. At first, the initial machine structure and rotor dimensions should be set and verified by mechanical analysis; then the machine power loss is estimated and processed by thermal analysis. The machine electromagnetic scheme should be adjusted until the satisfaction of mechanical and temperature requirements.

Surface-mounted and interior PM structures are two rotor options for PMSMs. The latter has a higher power density, while surface-mounted PM structure is considered to be a better choice for high speed applications as it can withstand more stress resulting from high speed rotation. A good choice of PM material is also desirable for high speed PMSMs: SmCo can withstand the temperature up to 350 °C, while NdFeB has the advantages of higher coercive force with larger remanence. Moreover, the mechanical performance of NdFeB is also superior to SmCo as this is important for high speed operation. Therefore, an NdFeB-based surface mounted PMSM is chosen in this research.

The pole number of high speed machines is usually 2 or 4. Although the electrical frequency for 2-pole machines can be lower, their end-winding length is longer than the 4-pole machines, which would deteriorate machine dynamic performance during high speed. As a result, a 4-pole structure is adopted.

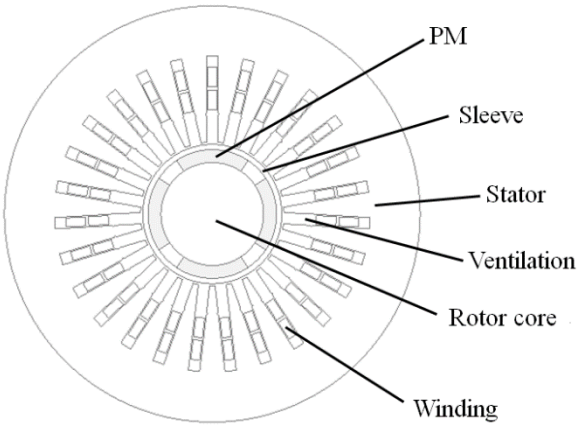

Fig. 1. High speed PMSM structure

In this paper, a 1 MW PMSM is developed to operate at the rated speed of 18, 000 rpm. Its structure is shown in Fig. 1 and its key parameters are listed in Table I. A rotor sleeve is employed to protect PMs from large centrifugal force due to high speed rotation. The sleeve is woven outside the PMs' outer surface by carbon fiber, and it is wound around the rotor layer by layer. The iron core is laminated in the axial direction while the PMs are magnetized in radial direction. There are two pieces of magnets along axial length for one pole to facilitate PM manufacture. The machine rotor is made of laminated iron to decrease rotor power loss.

TABLE I
High Speed PMSM Parameters

item	parameter	item	parameter
rated power	1 MW	rated speed	18 000 rpm
current amplitude	355A	rated frequency	600 Hz
stator outer diameter	550 mm	stator bore diameter	190 mm
rotor outer diameter	184 mm	air gap length	3 mm
iron core length	400 mm	slot number	27
pole number	4	PM material	NdFeB
PM thickness	17 mm	PM conductivity	625000 S/m
winding layers	2	conductors per slot	6

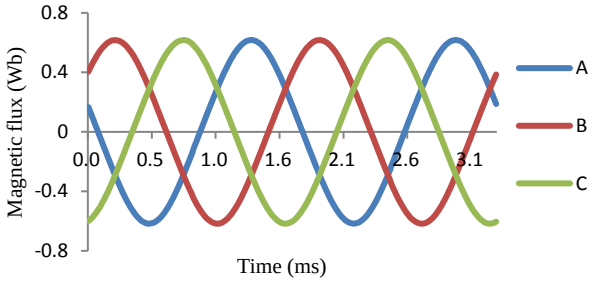

Fig. 2. Magnetic flux

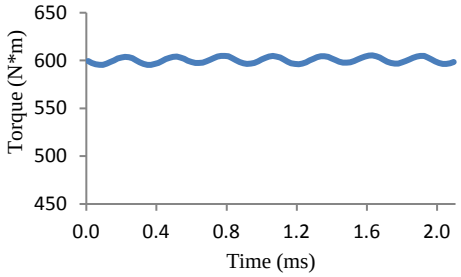

Fig. 3. Output torque at full load

Fig. 2 shows the windings magnetic flux for the machine at rated speed with no load, while Fig. 3 presents the machine output torque at full load with rated speed analyzed by FEM.

A deep slot structure is adopted in the high speed PMSM stator as the ventilation region for rotor cooling. Deep slot structure also gives rise to slot leak inductance. For the high speed PMSM researched, the slot leak inductance is 0.643 mH.

III. Power Loss Analysis

A. Iron Loss Analysis

Iron loss accounts for considerable proportion in the whole power loss as the frequencies in high speed machines are much higher than conventional ones. Generally, Iron loss in the steel core can be estimated by adding the hysteresis loss P_h, eddy current loss P_e and anomalous loss P_a in conventional method as [19]:

$$P_{fe} = P_h + P_e + P_a = k_h \cdot f \cdot B_m^2 + k_e \cdot f^2 \cdot B_m^2 + k_a \cdot f^{1.5} \cdot B_m^{1.5} \quad (1)$$

where k_h, k_e, k_a are the hysteresis loss coefficient, eddy current loss coefficient and anomalous loss coefficient, respectively. k_a is so small for high grade steel utilized in the high speed PM machine of this paper which can be neglected; f is the frequency and B_m is the flux density magnitude.

As the magnetic flux waveform in practical iron core is not exactly sinusoidal, the eddy current loss coefficient k_e is also a variable to frequency f [18]. Moreover, the additional iron loss due to rotational magnetic flux in the steel core is also necessary to consider in iron loss analysis. The magnetic flux variation at each point of the iron core is obtained; the radial and tangential components of the flux density fundamental and harmonics are resolved by Fourier analysis; then the flux vector trajectory ellipse for each harmonic can be obtained and the short axis and long axis can be worked out. The additional core loss caused by the rotational field is proportional to the circular degree of flux vector loci which is expressed by the short-axis-to-long-axis rate of flux vector ellipse. So the hysteresis loss and eddy current loss can be evaluated as:

$$P_h = \sum_{i=1}^{M} k_h(B_i) f_i (1 + \gamma D_i) \quad (2)$$

$$P_e = \sum_{i=1}^{M} k_e(B_i, f_i) f_i^2 (1 + \gamma D_i) \quad (3)$$

where f_i is the i order frequency, B_i is the magnetic flux density at f_i which is determined from Fourier analysis, $k_h(B_i)$ denotes the coefficient of magnetic flux density and $k_e(B_j, f_j)$ is the coefficient corresponding to frequency f_i, D_i is the rate of short axis to long axis of the flux vector trajectory ellipse at harmonic order i and γ is a coefficient to consider the iron loss due to rotational flux [20]. In this study, γ is taken as 0.96 based on iron core manufacture. Then the effects of high order harmonic components in the flux density and rotational flux can be taken into consideration for iron loss prediction.

Based on the improved iron loss estimation method, the iron loss for the machine at rated speed (18000 rpm) is 6116.8 W. The iron loss due to fundamental magnetic field is the major component up to 91.8% in the total iron loss, while the loss due to third order harmonic is 5.3% and it is 1.5% for fifth order harmonic, 1.1% for seventh order harmonic. The iron loss caused by high order flux density harmonic components account for about 8.8% of the iron loss due to fundamental component for the machine at rated speed. So the harmonic flux density components contribute considerable proportion in the iron loss of high speed PM machine.

Fig.4 presents a comparison of iron loss calculated by conventional method, the method considering harmonic components iron loss without rotational iron loss and the method considering both harmonics and rotational effects under different speeds. It can be seen that for the machine under rated speed, the iron loss considering only harmonic components is 1380 W less than the iron loss considering both harmonic and rotational loss effects, which accounts for about 20% in the total iron loss. So the PMSM core loss is affected not only by alternating flux effect but also rotational flux effect, and it is valuable to take both into consideration for PMSMs core loss estimation, especially for high speed applications.

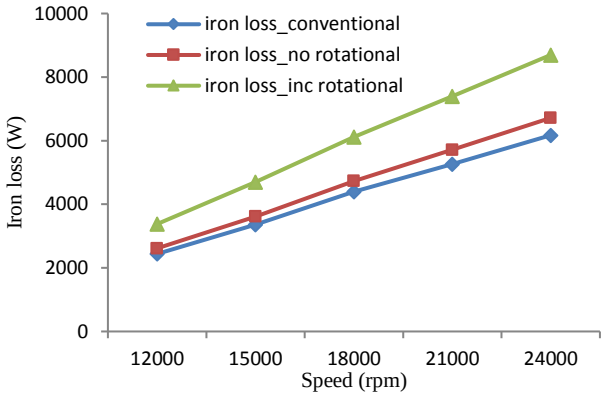

Fig. 4. Iron loss with machine speed

B. Rotor Eddy Current Loss

The rotor eddy current loss is critical in high speed PMSMs as it is only removed through the air gap. The induced eddy current density J in the rotor can be calculated from the waveform of the vector potential by performing a numerical time derivation [21] as:

$$J = -\frac{1}{\rho}\frac{\partial A}{\partial t} + c(t) \quad (4)$$

where A is the magnetic vector potential, ρ is the electrical resistivity and $c(t)$ is the function of time which guarantees a zero net current through rotor, and the rotor eddy current loss then can be obtained as:

$$p_e = \int_{rotor} \frac{J^2}{\sigma} dV \quad (5)$$

where σ is the conductivity and V is the rotor volume. In this paper, 2D time-stepping FEM (finite element method) is utilized with field- circuit coupling method adopted, the stator end winding resistance and leakage inductance can be considered by adding a corresponding resistance and inductance in the circuit. Therefore the rotor eddy current loss can be calculated as:

$$P_e = \frac{1}{k}\sum_{i=1}^{k}\sum_{e=1}^{m} J_{ie}^2 \Delta_e \sigma^{-1} l \quad (6)$$

where J_{ie} is the eddy current density in the element e at step i, Δ_e is the element area, k is the step number and m is the element number while l is the rotor length [14].

As the PM has a low mechanical tensile capability, the rotor sleeve is always utilized to protect the surface-mounted PMs against the centrifugal force during high speed operation. However, the rotor sleeve itself can impact on the electromagnetic performance of the PMSM. In this paper, three materials, carbon fiber (conductivity: 2.20×10^4 S/m), Ti alloy (conductivity: 5.05×10^5 S/m) and copper (5.98×10^7 S/m), are considered for the rotor sleeve. Their rotor eddy current density distributions of the machine at rated speed are shown in Fig.5.

It can be observed that the eddy current distribution is greatly influenced by the sleeve conductivity: the eddy current density is distributed all over the rotor, and the highest eddy current density area occurs at PMs which is up to 2.60×10^6 A/m^2 for the carbon fiber sleeve; the eddy current is mostly distributed on the rotor sleeve, and the eddy current in PMs is effectively reduced if adopting the Ti- alloy sleeve; since copper has much higher conductivity than PMs, the harmonics can hardly reach PMs while the eddy current density is mainly distributed on the copper sleeve surface (up to 2.05×10^8A/m^2). Such a high eddy current density would result in excessive rotor eddy current loss if utilizing high conductivity rotor sleeve. However, it should be pointed out that the metal rotor sleeve with high conductivity normally also has much higher thermal conductivity than carbon fiber, which is helpful in rotor thermal dissipation. Although metal rotor sleeves can be found application in high speed PM machines, this work considers carbon fiber as rotor sleeve.

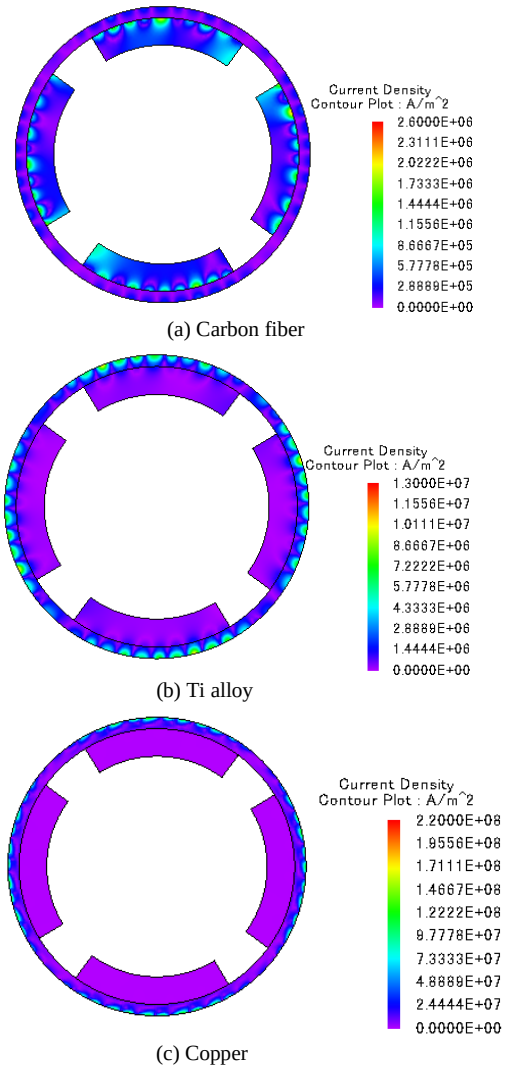

(a) Carbon fiber

(b) Ti alloy

(c) Copper

Fig. 5. Eddy current density distribution for different sleeve material

Table II compares the rotor eddy current loss calculated by FEM for the high speed PMSM with different stator slot number at rated operation condition. All the machines have the same stator slot opening width, while windings and iron core lengths are slightly adjusted to maintain the same output torque of the machines. It can be found that rotor eddy current loss is significantly reduced with stator slot number rises. As machine stator slot number has a critical impact on machine magnetic field harmonics, a multi-slot stator structure is preferred for high speed PMSM design to decrease rotor eddy current loss effectively.

TABLE II
HIGH SPEED PMSM PARAMETERS

Slot number	18	24	27
Sleeve (W)	2567.1	2264.9	1571.3
PM (W)	3403.6	1192.1	1110.4
Total (W)	5970.7	3457.0	2681.7

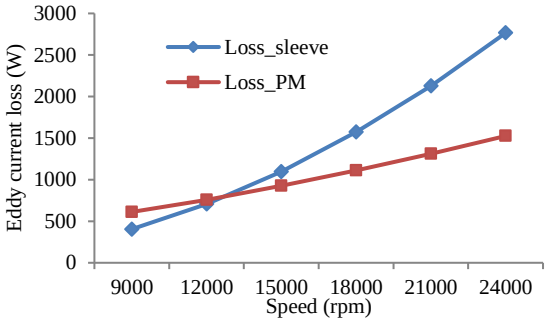

Fig. 6. Eddy current loss with machine speed

Fig. 6 shows the rotor eddy current loss of the sleeve and PMs for the high speed PMSM with carbon fiber rotor sleeve at different machine speeds. It is notable that the sleeve loss is nearly proportional to the speed squared, while the loss in PMs does not increase quite much with rotor speed rising. In the low conductivity case of carbon fiber, the induced eddy current is not large enough to influence the magnetic field in sleeve. So the eddy current is nearly proportional to the speed and the eddy current loss is almost proportional to the speed squared. Since PMs have high conductivity, considerable eddy current can be induced on PM's top side, and it can effectively prevent magnetic field harmonics further entering into PMs. So the PMs eddy current loss increases with a relatively slow rate when machine speed rising.

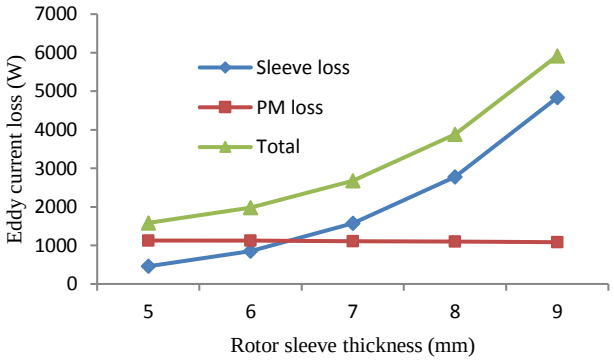

Fig. 7. Rotor eddy current loss with sleeve thickness

Fig. 7 presents the rotor eddy current loss as a function of the carbon fiber sleeve thickness, while the distance between the stator inner diameter and the PM outer diameter is fixed at

10 mm during calculation for the high speed PMSM at the rated speed (18000 rpm) with rated load. As the rotor sleeve thickness increases, the total rotor eddy current loss increased dramatically since the harmonics effect is strengthened with reduced air gap. Therefore it is favorable to adopt a thin rotor sleeve to decrease rotor eddy current loss where mechanical requirements allow. The PM eddy current loss only got slightly decreased with sleeve thickness variation. It can be explained as the shielding effect from carbon fiber sleeve is low, and the harmonics penetration depth in sleeve is much higher than the sleeve thickness, while the magnetic harmonics do not get effectively restrained through sleeve and the PMs magnetic field do not change quite much. So the sleeve thickness has quite limited effect in PM eddy current loss variation. Table III further compares the eddy current loss with sleeve conductivity (sleeve thickness 7mm) for the machine with rated speed at rated load, it can be observed that the total rotor eddy current loss increases along with sleeve conductivity, and it is beneficial to utilize low electrical conductivity sleeve to decrease eddy current loss.

TABLE III
EDDY CURRENT LOSS WITH SLEEVE CONDUCTIVITY

Conductivity(*10^4S/m)	1	2	3	4	5
Sleeve (W)	732.3	1456.9	2177.0	2891.6	3600.5
PM (W)	1137.4	1122.0	1106.9	1092.2	1077.8
Total (W)	1869.7	2578.9	3283.9	3983.8	4678.3

As analyzed previously, the copper sleeve with high conductivity can offer dramatic shielding effect to PMs and stop harmonics penetrating into PMs. Then a composite rotor sleeve structure is studied to decrease the eddy current loss in PMs as shown in Fig.8 (a), while (b) presents the flux line distribution in the machine at rated condition with 1.2 mm copper shield:

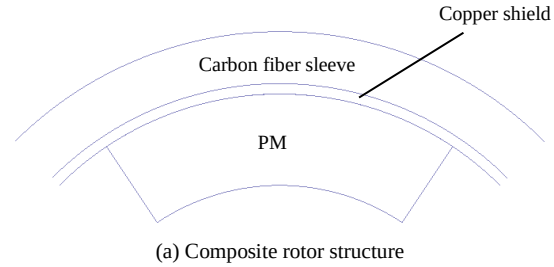

(a) Composite rotor structure

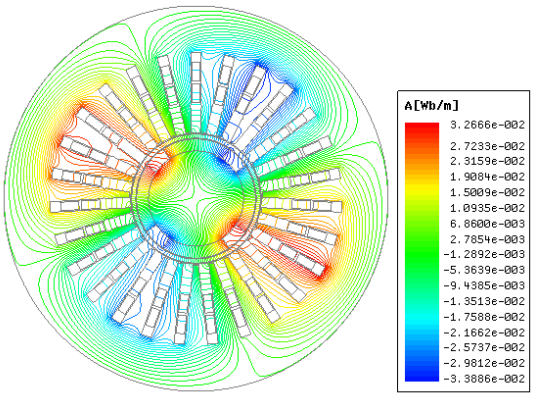

(b) Flux line distribution

Fig. 8. Composite rotor

A copper shield is added between the carbon fiber sleeve and PMs, while the relation between rotor eddy current loss and copper shield thickness is tabulated in Table IV for the machine with a fixed 3-mm air gap length at rated operation:

TABLE IV
EDDY CURRENT LOSS UNDER DIFFERENT COPPER SHIELD THICKNESS

Copper shield thickness (mm)	PM (W)	Shield (W)	Sleeve loss (W)	Total (W)
0	1110.4	-	1571.3	2681.7
0.3	142.8	2612.8	1377.9	4133.5
0.6	47.1	2180.2	1320.7	3548.0
0.9	25.5	1981.4	1280.8	3287.7
1.2	19.0	1966.1	1242.9	3228.0
1.5	23.4	2113.6	1203.3	3340.3
1.8	32.3	2410.5	1159.5	3602.3

It can be seen that the PM eddy current loss is effectively decreased with the added copper shield, and the sleeve loss also decreases with the copper shield thickness. However, the shield loss and total rotor eddy current loss witness a deduction at first, and then increase when the copper shield gets thicker. The minimal total eddy current loss is found when the copper shield thickness is 1.2 mm, but the total rotor eddy current loss is still higher than that without a copper shield. However, copper has relatively large thermal conductivity, which is beneficial in rotor thermal dissipation; moreover, the composite rotor structure can also impact the machine anti-demagnetization capability, and it will be illustrated in section IV.

C. Windage Loss

The windage loss is due to the air friction when the rotor rotates and it becomes significant as the machine speed increases. The rotor can be approximately modeled as a cylinder with its windage loss analytically calculated by means of [16]:

$$P_{windage} = C_f \pi \rho \omega^3 r^4 l \qquad (7)$$

where ρ denotes air gap density, ω is the angular speed, r, l are the rotor radius and length respectively, while C_f is the friction coefficient which is relevant to the air gap structure and rotor surface condition. As the analytical calculation method is based on several empirical coefficients, alternatively, the air gap friction loss can be calculated more accurately through fluid field analysis. Fig.9 shows the ventilation model for the high speed PMSM: the groove in the model is the ventilation region in the stator slots as shown in Fig.1.

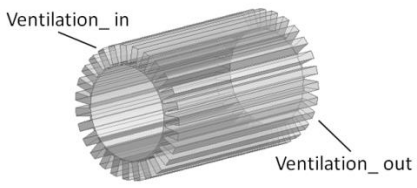

Fig. 9. Air gap and ventilaition groove model

Fig. 10 shows the relationship between windage loss under different rotor speed and rotor roughness height, while Fig. 11 displays the comparison of windage loss under different axial

air ventilation speeds for the machine with rated speed. It can be found the windage loss is nearly as a relation of exponential manner with rotor speed, which can be dramatically increased with the machine speed rise. The rotor surface roughness is also a critical factor: the windage loss also gets increased with rough rotor surface. Moreover, though the axial ventilation path is beneficial to decrease the machine temperature, an extra windage loss is also added to the total loss. Thus it is advantageous to use a sleeve material with a smooth surface and operate a suitable ventilation speed for high speed PMSMs.

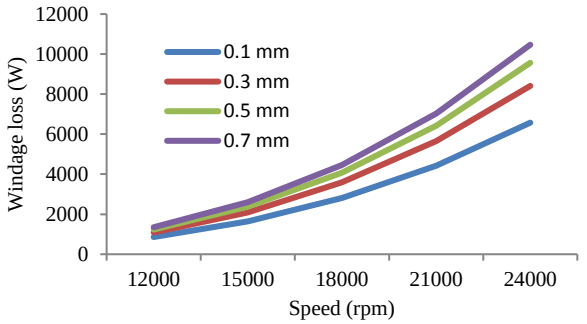

Fig. 10. Relationship between windage loss and rotor speed with rotor roughness height

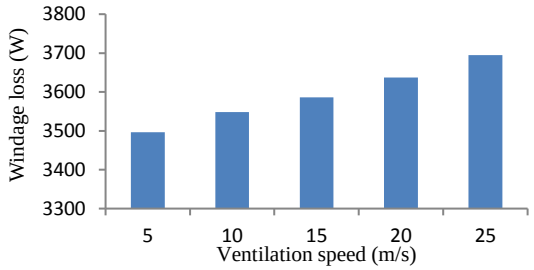

Fig. 11. Windage loss with ventilation speed

IV. Demagnetization Analysis

The demagnetization of PMs may occur due to high temperature and armature reaction. The demagnetization curve for NdFeB (NEOMAX-38H) is shown in Fig.12: if the flux density in PMs is below the knee point (point A), the PM remanence would change from the origin point (R) to a new point (R') through the recoil line. In this paper, the PM demagnetization is assessed by the demagnetization ratio, which is defined as the ratio of residual flux density loss after demagnetization to the original PM residual flux density.

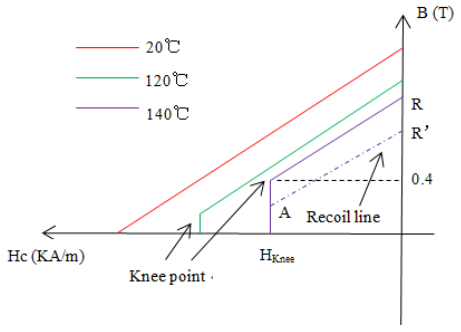

Fig. 12. PM demagnetization curve with temperature

The demagnetization due to temperature is performed on machine over load condition as the high speed PMSM powered by twice rated current in amplitude, while Fig.13 shows the demagnetization ratio of the PMs under different temperatures. As can be found, no demagnetization occurs when the operational temperature is 100 °C; partial demagnetization takes place on the PM edge when the temperature increases to 120 °C; and it becomes more severe on the PM corners if the temperature rises to 140 °C and 160 °C due to magnetic reaction flux concentrates on the corners. The winding current also has a critical effect on PM demagnetization. Fig.14 demonstrates the output torque under different current excitations (1.5, 2, 3, 4 times of rated current in amplitude) with the temperature varies as: firstly the original operational temperature is 60 °C, then it increase to 140 °C at 0.008 s and next sets back to 60 °C again at 0.02 s. Clearly, the torque can return to its initial value when the PMSM is powered by a current of 1.5 times the rated; while the recovered torque is lower than its initial value with a larger current. Moreover, the recovered torque at the 3-times rated current is close to that at the 4-times rated current, indicating considerable demagnetization occurs when 3-times rated current is applied to the PMSM under 140 °C.

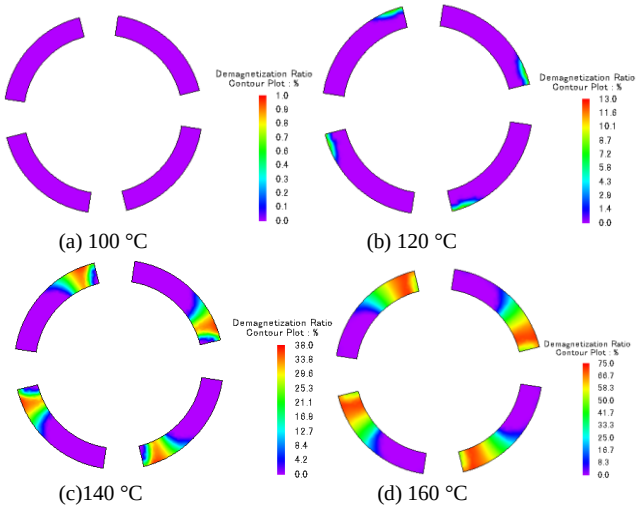

Fig. 13. Demagnetization ratio with temperature

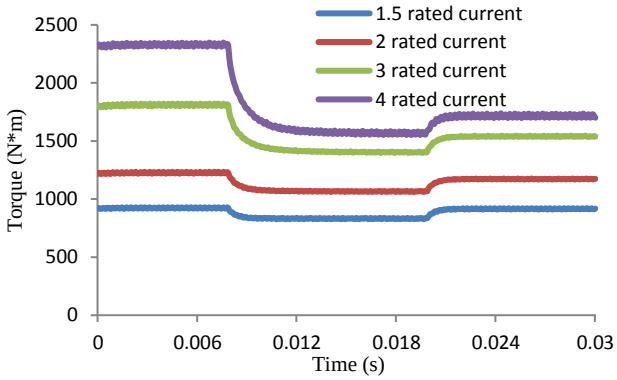

Fig. 14. Torque under winding current

Fig.15 compares the back electromotive force (EMF) waveform upon the demagnetization effect raised by the over current in amplitude of the stator winding at 140 °C. As can be found not only the EMF amplitude got decreased, the EMF waveform also got distorted after demagnetization.

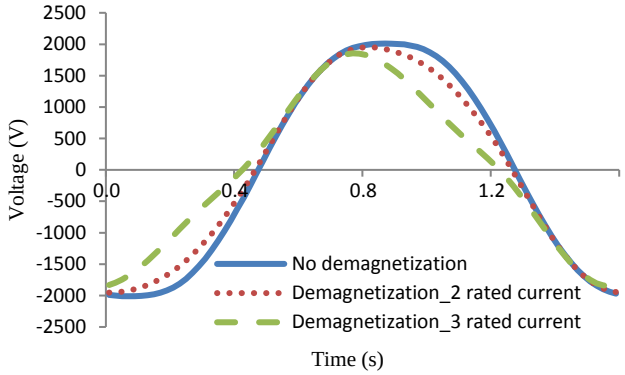

Fig. 15. Back EMF waveform after demagnetization

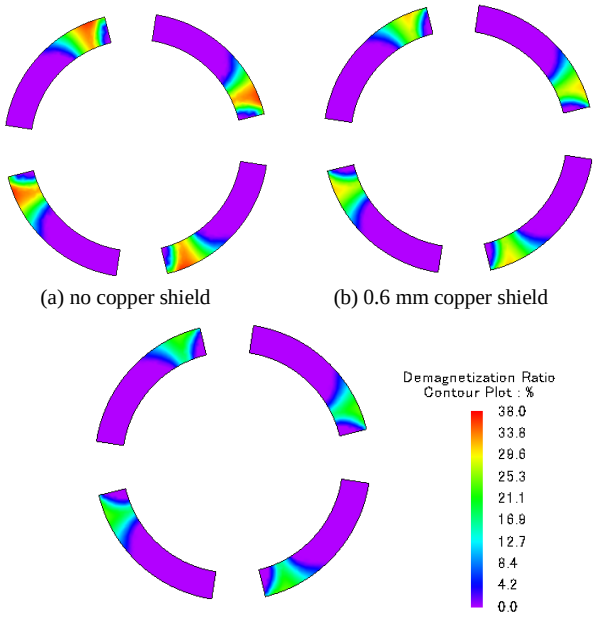

(a) no copper shield (b) 0.6 mm copper shield

(c) 1.2 mm copper shield

Fig. 16. Demagnetization analysis

Fig.16 displays the PM demagnetization comparison between the rotor without copper shield and composite rotor structure with copper shield on machine harsh condition as twice rated current amplitude applied to windings at 140 °C. It can be observed that composite rotor structure can decrease the exterior magnetic field effect to PMs due to the magnetic shielding effect from the copper layer, and reduce the demagnetization level and demagnetization area at harsh conditions. So the composite rotor structure with copper shield can effectively improve the machine anti-demagnetization capacity.

V. Thermal Analysis

The CFD model for the high speed PMSM is constructed to investigate the cooling ventilation and temperature distribution by electro thermal-fluid coupling analysis. The electromagnetic losses are regarded as heat sources for thermal analysis, while the forced air cooling is adopted via the air blown axially into the machine from one end to facilitate winding and rotor heat dissipation. Furthermore, the circumferential groove is also ducted around the machine frame for water cooling. Only 1/27 of the machine is modeled with periodic boundaries applied, while rotor rotation is considered by setting moving wall conditions at rated speed on the rotor surface. Standard K-ε model is adopted for turbulent flow calculation with viscous dissipation term included in energy equation to consider the air drag effect for the rotor under high speed operation. The iterative process is also adopted during the electro thermal-fluid coupling analysis to include the influence of machine operational temperature on the machine electromagnetic performance, as the machine material electromagnetic properties vary with operational temperatures. Firstly the losses of the different components in machine at initial temperature T_k are obtained through electromagnetic analysis which is next sent to CFD fluid-thermal analysis as heat source; then a new calculated temperature T_{k+1} can be determined by CFD while the machine components' material electromagnetic properties are replaced with new ones at the working temperature T_{k+1} for the next coming electromagnetic analysis; the electro thermal-fluid analysis is processed iteratively until the maximum temperature difference between T_{k+1} and T_k is less than a preset requirement.

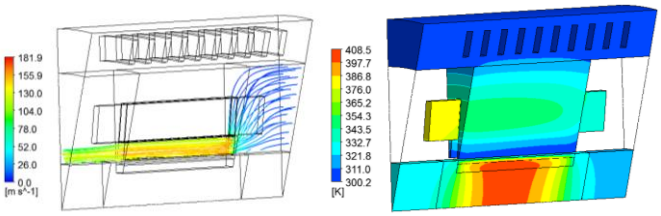

(a) Velocity streamline (b) Temperature field distribution

Fig. 17. CFD results of the high speed PMSM under rated condition

Fig.17 presents the CFD calculation results of the high speed PMSM at rated load condition. As can be found, the highest temperature of the machine occurs in the middle of the rotor and gradually dropped to both ends, while the highest spot of the winding and stator are located near the outlet of the cooling air. Both water cooling and air cooling can effectively act to constrain the machine temperature rise in its components.

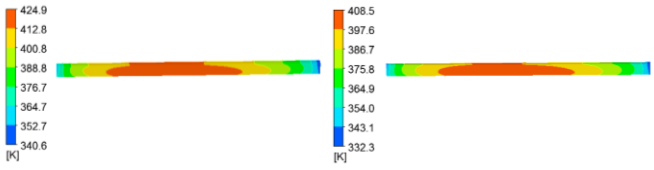

(a) 5m/s (b) 10m/s

Fig. 18. Temperature distribution for PM under different air flow rates

Fig. 18 further compares the PM temperature with different

air flow rates: the increase of air speed can obviously decrease the PM temperature, as the temperature is 424.9 K (151.7 ℃) in PM when air flow rate is 5 m/s, while it drops to 408.5 K (135.3 °C) when the air flow rate increases to 10 m/s. So increase the ventilation air flow rate in moderate degree is an effective method to reduce the PM temperature for the machine during high speed operation.

VI. Experimental Tests

The MW high speed PMSM is prototyped and experimentally tested. The stator core with windings and the rotor of the high speed PMSM are shown in Fig. 19 (a) and (b), respectively.

(a) Stator with windings (b) Rotor

Fig. 19. Stator and rotor for high speed PMSM

Fig. 20 shows the no-load line-line EMF waveforms of the high speed PMSM at rated speed from FEM and experimental tests. Clearly, numerical and experimental results have a good agreement on the EMF.

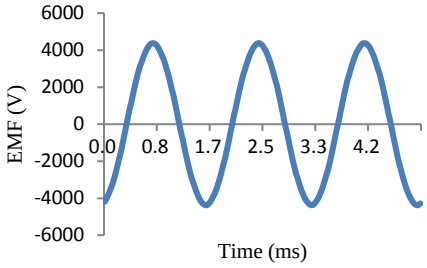

(a) EMF by FEM

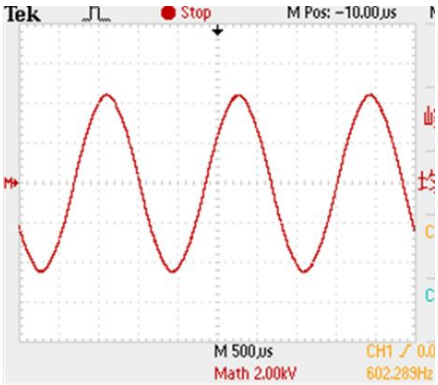

(b) EMF (2 kV/grid) by measurement

Fig. 20. Line-line EMF

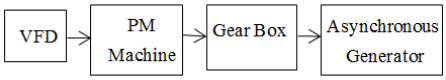

(a) Load test scheme

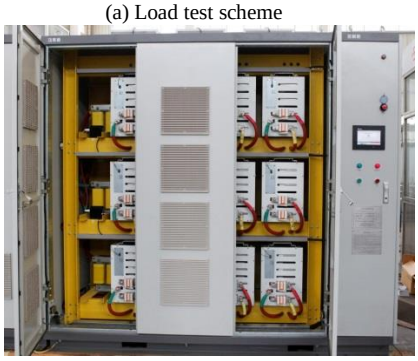

(b) Nine-level high voltage inverter

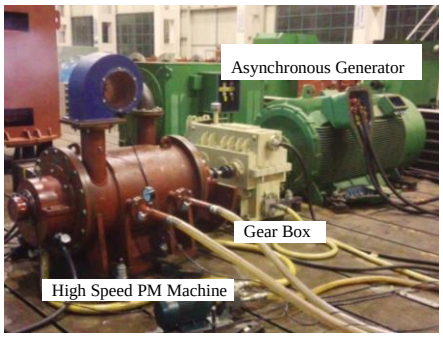

(c) Load test

Fig. 21. Load test for high speed PM machine

The load tests for the developed high speed PMSM are based on the scheme as shown in Fig.21 (a): the machine is powered by variable frequency drive (VFD) with voltage, it drives an asynchronous generator and the coupling between the two machines is achieved by means of gear box. So the high speed PMSM output can be reflected by the power generated by asynchronous generator. VFD is a nine level high voltage inverter with vector control method applied to achieve control in both machine speed and power during high speed operation. The nine level high voltage inverter (as shown in Fig.21 (b)) has advantage of powering the machine with low harmonics, and it is a desirable solution for high power rate high speed machine drive. While Fig 21 (c) displays the test rig of the load test for high speed PMSM. Fig. 22 presents the winding phase current of the machine at rated speed (18000 rpm) and rated load condition. The measured power factor is 0.966. The winding currents are shown as sinusoidal waveform and the measurement result agrees well with numerical result from the FEM calculation.

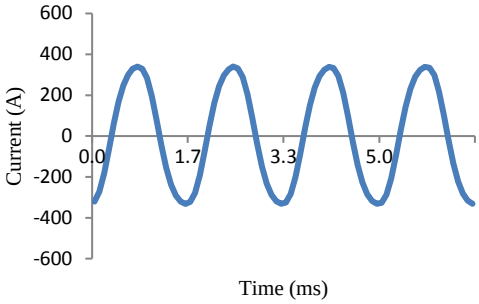

(a) Winding phase current by FEM

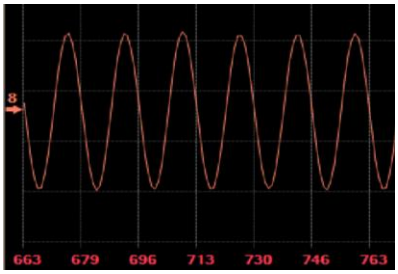

(b) Winding phase current by measurement (200A/grid)

Fig. 22. Phase current for the high speed PM machine at rated load

Table V and VI present the experiment test results of the whole high speed PMSM system performance with different load applied. The input power to VFD and the output power of asynchronous generator are measured when the PMSM operates at 10,200 rpm and 18,000 rpm respectively. Considering the results listed are for the whole test system including gear box, it can be concluded from the measurements that the designed high speed PM machine has a desirable performance.

TABLE V EXPERIMENT MEASUREMENT WITH THE PM MACHINE AT 10200 RPM UNDER DIFFERENT LOAD

VFD			Asynchronous Generator		
Voltage (V)	Current (A)	Power (kW)	Voltage (V)	Current (A)	Power (kW)
9867	9.0	149.6	1758	45.6	113.5
9744	15.2	250.7	2395	61.8	213.1
9800	21.1	349.3	2882	74.3	306.8
9805	27.0	445.7	3000	89.4	399.4
9720	36.6	595.8	3115	113.0	535.7

TABLE VI EXPERIMENT MEASUREMENT WITH THE PM MACHINE AT 18000 RPM UNDER DIFFERENT LOAD

VFD			Asynchronous Generator		
Voltage (V)	Current (A)	Power (kW)	Voltage (V)	Current (A)	Power (kW)
9535	33.5	535.4	3516	82.6	423.8
9572	40.2	643.2	3488	101.2	516.0
9482	50.8	803.5	3490	129.6	654.0
9585	56.5	903.1	3499	147.7	735.9
9527	63.0	999.6	4018	140.4	835.0
9534	63.2	1003.8	4016	140.8	836.7
9924	69.3	1146.0	3981	157.7	921.5

In order to verify the temperature field prediction, the temperature resister detectors are installed in the winding and stator yoke at air flowing inlet and outlet sides respectively. The prototype machine is tested under the rated conditions (current and speed). Fig.23 shows the temperature measurement device. During the test, the machine is operated at rated conditions and reaches a steady state. Then the related temperatures are recorded for further comparison. As shown in Table VII, the temperature of winding and stator near air floating outlet is higher than that near inlet, and the predicted values from CFD analysis are very close to the measured temperatures. Overall the experimental tests have validated the developed numerical models in predicting key power losses in the machine.

Fig. 23. Temperature measurement device

TABLE VII
TEMPERATURE FOR HIGH SPEED PM MACHINE (°C)

	Inlet		Outlet	
	Winding	Stator yoke	Winding	Stator yoke
CFX	65.3	52.1	110.3	62.5
Measurement	68.8	55.8	114.5	66.2

VII. CONCLUSION

In this paper, a MW level high speed PMSM is analyzed with detailed electromagnetic and thermal performance. Iron loss is calculated based on an improved method. It can be found that harmonics and rotational magnetic field effects should be considered in high speed PMSM iron loss estimation for higher precision. Rotor eddy current loss performance is discussed and illustrated with machine structure and rotor sleeve impacts. Eddy current loss can be decreased by multi-slot stator structure, while application of low conductivity and thin sleeve with permission of mechanical constraints could also be helpful to reduce the total rotor eddy current loss. The mechanical friction loss is also estimated with reasonable accuracy. The PMs demagnetization causes degradation in machine performance, and a composite rotor structure is proposed to effectively improve the machine's anti-demagnetization capacity under harsh operation conditions. The temperature distribution of the high speed PMSM under rated condition is calculated based on fluid-thermal coupling analysis by CFD, and the reduction in the rotor temperature rise can be achieved by axial air cooling ventilation. The research and effectiveness of the FEM and CFD models have been verified by experimental measurements on a prototype machine.

VIII. REFERENCES

[1] D. Gerada, A. Mebarki, N. Brown, C. Gerada, A. Cavagnino and A. Boglietti, "High-speed electrical machines: technologies, trends, and developments," *IEEE Trans. Industrial Electronics*, vol. 61, no. 6, pp. 2946–2959, Jun. 2014.

[2] Z. Konlondzovski, A. Arkkio, J. Larjola and P. Sallinen, "Power limits of high speed permanent magnet electrical machines for compressor applications," *IEEE Trans. Energy Conversion*, vol. 26, no. 1, pp. 73–82, Mar. 2011.

[3] N. Uzhegov, E. Kurvinen, J.Nerg, J. Pyrhonen, J. Sopanen and S. Shirinskii"Multidisciplinary design process of a 6-slot 2-pole high speed permanent-magnet synchronous machine," *IEEE Trans. Industrial Electronics*, vol. 63, no. 2, pp. 784–795, Feb. 2016.

[4] J. Kim, I. Jeong, K. Nam, J. Yang and T. Hwang, "Sensorless control of PMSM in a high speed region considering iron loss," *IEEE Trans. Industrial Electronics*, vol. 62, no. 10, pp. 6151–6159, Oct. 2015.

[5] S. Jang, H. Cho, S. Lee H. Yang and Y. Jeong, "The influence of magnetization pattern on the rotor losses of permanent magnet high speed machines," *IEEE Trans. Magnetics*, vol. 62, no. 10, pp. 6151–6159, Oct. 2015.

[6] Z. Kolondzovski, A. Belahcen and A. Arkkio, "Comparative thermal analysis of different rotor types for a high speed permanent magnet electrical machine," *IET Electric Power Applications* vol. 3, no. 4, pp. 279–288, Apr. 2008.

[7] Z. Huang, J. Fang, X. Liu and B. Han, "Loss calculation and thermal analysis of rotor supported by active magnetic bearings for high speed permanent magnet electrical machines," *IEEE Trans. Industrial Electronics*, vol. 63, no. 4, pp. 2027–2035, Apr. 2016.

[8] Y. Huang, J. Dong, J. Zhu and Y. Guo, "Core loss modeling for permanent magnet motor based on flux variation locus and finite element method," *IEEE Trans. Magnetics*, vol. 48, no. 2, pp. 1023–1026, Feb. 2012.

[9] S. Zhu, M. Cheng, J. Dong and J. Du, "Core loss analysis and calculation of stator permanent magnet machine considering DC-biased magnetic induction," *IEEE Trans. Industrial Electronics*, vol. 61, no. 10, pp. 5203–5212, Oct. 2014.

[10] J. Seo, D. Woo, T. Chung and H. Jung, "A study on loss characteristics of IPMSM for FCEV considering ," *IEEE Trans. Magnetics*, vol. 46 no. 8, pp. 3213–3216, Aug. 2010.

[11] J. Seo, T. Chung, C. Lee, S. Jung and H. Jung, "Harmonic iron loss analysis of electrical machines for high speed operation considering driving condition," *IEEE Trans. Magnetics*, vol. 45, no. 10, pp. 4656–4659, Oct. 2009.

[12] Z. Zhu, K. Ng, N. Schofield and D. Howe, "Improved analytical modeling of rotor eddy current loss in brushless machines equipped with surface-mounted permanent magnets," *IEE Proceedings*, vol. 151, no. 6, pp. 641–650, Nov. 2004.

[13] D. Ishaak, Z. Zhu and D. Howe, "Eddy-current loss in the rotor magnets of permanent magnet brushless machines have a fractional number of slots per pole," *IEEE Trans. Magnetics*, vol. 41, no.9, pp. 2462–2469, Sep. 2005.

[14] W. Li, H. Qiu, X. Zhang and R. Yi, "Influence of copper plating on electromagnetic and temperature fields in a high speed permanent magnet generator," *IEEE Trans. Magnetics*, vol. 48, no.8, pp. 2247–2253, Aug. 2012.

[15] J. Shen, H. Hao, M. Jin and C. Yuan, "Reduction of Rotor Eddy Current Loss in High Speed PM Brushless Machine by Grooving Retaining Sleeve," *IEEE Trans. Magnetics*, vol. 49, no.7, pp. 3973–3976, Jul. 2013.

[16] J. Xing, F. Wang, T. Wang and Y. Zhang, "Study on anti-demagnetization of magnet for high speed permanent magnet machine," *IEEE Trans. Applied superconductivity*, vol. 20, no. 3, pp. 856–860, Jun. 2010.

[17] J. Dong, Y. Huang, L. Jin, B. Guo, H. Lin, J. Dong, M. Cheng and H. Yang, "Electromagnetic and thermal analysis of open-circuit air cooled high-speed permanent magnet machines with gramme ring windings," *IEEE Trans. Magnetics*, vol. 50, no. 11, pp. 1–4, Nov. 2014.

[18] J. Dong, Y. Huang, L. Jin, H. Lin and H. Yang, "Thermal optimization of a high speed permanent magnet motor," *IEEE Trans. Magnetics*, vol. 50, no. 2, pp. 1–4, Feb. 2014.

[19] Z. Zhang, L. Yu, L. Sun, L. Qian and X. Huang, "Iron loss analysis of doubly salient brushless DC generators," *IEEE Trans. Industrial Electronics*, vol. 62, no. 4, pp. 2156–2163, Apr. 2015.

[20] L. Ma, M. Sanada, S. Morimoto and Y. Takeda, "Prediction of iron loss in rotating machines with rotational loss included," *IEEE Trans. Magnetics*, vol. 39, no. 4, pp. 2036–2041, Jul. 2003.

[21] L. Papini, T.Raminosoa, D. Gerada and C. Gerada, "A high speed permanent magnet machine for fault tolerant drivetrains," *IEEE Trans. Industrial electronics*, vol. 61, no. 6, pp. 3071–3080, Jun. 2014.